Advances in Science and Technology Research Journal

Advances in Science and Technology Research Journal, 2026, 20(6), 247–261
https://doi.org/10.12913/22998624/217610
ISSN 2299-8624, License CC-BY 4.0

Received: 2026.01.06
Accepted: 2026.04.15
Published: 2026.05.01

A dual-response optimization framework for fused deposition modeling printed polyethylene terephthalate glycol: Integrating surface finish and tensile-yield strength via response surface methodology

Ema Mastura Manika Mustaffa[1], Martini Muhamad[1*], Muhammad Khalil Zakaria[2], Yew Been Seok[1], Nurul Nnadiah Zakaria[3]

[1] Faculty of Innovative Design and Technology, Universiti Sultan Zainal Abidin, Gong Badak Campus, 21300 Kuala Terengganu, Malaysia
[2] My AZ Resources Sdn. Bhd., No. 33A-2, Jalan Impian Mahkota 1, Saujana Impian, 43000, Kajang, Selangor, Malaysia
[3] Manufacturing and Management Technology Section, Malaysia Italy Design Institute, Universiti Kuala Lumpur, Malaysia
* Corresponding author's e-mail: martinimuhamad@unisza.edu.my

ABSTRACT

Additive manufacturing (AM), specifically fused deposition modelling (FDM), has emerged as a crucial fabrication method for polymer components because of its design versatility, material efficiency, and appropriateness for quick prototype and functional part production. Polyethylene terephthalate glycol (PETG) is extensively utilised in FDM applications due to its advantageous thermal stability, dimensional precision, and mechanical properties. Nonetheless, the surface quality and mechanical properties of FDM-printed PETG components are significantly influenced by processing conditions, constraining their wider use in load-bearing and functional applications. This work seeks to systematically optimise critical FDM printing parameters to enhance surface finish and tensile strength in PETG components. A systematic experimental approach was employed to determine process–property correlations. Two experimental phases were executed. The initial phase examined the effects of layer height, nozzle temperature, and bed temperature on surface roughness. The second phase investigated the relationship between surface features and mechanical performance by assessing the tensile properties of PETG specimens printed with various infill patterns, specifically rectilinear, concentric, and octagram spiral, as well as differing construction orientations. A design of experiments (DOE) methodology utilising response surface methodology (RSM) was implemented to create predictive models, with the significance of parameters and model adequacy assessed through analysis of variance (ANOVA). The investigation confirmed strong anisotropy where the layer height significantly affected roughness at 90° ($p=0.03388$), but no significant model was found for 0° within the tested ranges. Surface roughness (Ra) ranged from 1.76 µm (minimum) to 5.81 µm (maximum) at 0° and from 6.29 µm to 11.70 µm at 90°. Mechanical testing demonstrated that tensile strength is significantly affected by infill pattern and build orientation. The concentric infill design demonstrated superior tensile strength, approximately 67% higher than the octagram spiral, due to improved load distribution and inter-filament continuity, whereas the rectilinear pattern provided an advantageous equilibrium among mechanical performance, material efficiency, and decreased printing duration. In all configurations, specimens produced with a 90° construction orientation exhibited enhanced tensile performance. This research presents a multi-parameter optimization and prediction framework for PETG FDM printing, facilitating tailored parameter selection to achieve an equilibrium among surface quality, mechanical performance, and production efficiency. The results validate the high-performance PETG components for functional-industrial AM applications.

Keywords: 3D-printing, polyethylene terephthalate glycol, design of experiment, ANOVA, surface roughness, tensile strength.

INTRODUCTION

The rapid integration of AM, especially FDM, in high-value sectors, from medical devices to functional prototypes, necessitates a transition from basic geometric fabrication to the dependable manufacturing of end-use components [1]. This transition depends on the reliable mechanical performance and surface quality of printed components. A persistent "process-structure-property" gap remains a significant impediment. Suboptimal printing parameters result in variable part quality, causing material, energy, and time wastage due to unsuccessful builds and post-processing demands. Thus, systematic parameter optimisation has transitioned from a specialised research focus to an industry necessity aimed at reducing resource consumption, minimising repeated trial-and-error, and maximising the potential of FDM for load-bearing applications [2].

Among the FDM material options, PETG has surfaced as a significant alternative to connect the prevalent polylactic acid (PLA) and engineering-grade acrylonitrile butadiene styrene (ABS). PETG is a modified type of PET enhanced with glycol to augment formability, chemical resistance, and durability, rendering it extensively utilised as an FDM filament for functional components and prototyping [3]. FDM constructs components layer by layer; therefore, process variables significantly affect interlayer adhesion, surface topography, and overall mechanical performance. Hence, systematic parameter investigations and optimizations are prevalent in PETG research [4]. In addition, it presents a compelling combination of attributes: enhanced toughness and impact resistance relative to PLA, improved chemical resistance, reduced warping propensity and odour release compared to ABS, and exceptional optical clarity. These characteristics render PETG more appropriate for applications necessitating durability, including specialised jigs, fittings, protective housings, and biological guides. Nonetheless, its mechanical and aesthetic capabilities are significantly influenced by the settings of the FDM process, which dictate layer adhesion, crystallisation characteristics, and surface morphology [5].

Comprehensive studies have demonstrated the fundamental impact of FDM settings on the characteristics of different polymers. Significant research has shown that factors including layer height, nozzle temperature, printing speed, infill density/pattern, and raster orientation significantly influence tensile strength, flexural modulus, and impact resistance [6–8]. For example, elevated nozzle temperatures typically enhance interlayer diffusion in semi-crystalline polymers, whereas reduced layer heights can increase resolution, albeit at the expense of build time. Literature has commenced delineating the behavioural characteristics of PETG. Research conducted by Kumaresan and Valvez has established that the mechanical properties of PETG are significantly influenced by temperature conditions, owing to its glass transition and crystallisation kinetics [9, 10]. Moreover, studies have indicated that factors such as printing speed and fan cooling substantially affect layer adhesion and dimensional precision in PETG, setting its ideal processing parameters apart from those of other thermoplastics [11].

Table 1 summarizes key FDM parameters evaluated for PETG, standard ranges documented in the literature, and their noted directional impacts on surface and tensile properties. The table presents succinct parameter ranges and primary reported effects from various studies. Layer height is consistently identified as the primary factor influencing surface roughness, whereas infill geometry/density and nozzle temperature frequently govern tensile properties [3, 4, 12–16].

Previous works have also been done on optimization studies that concurrently address surface and mechanical properties on PETG FDM. The quest for high-performance 3D-printed PETG components entails navigating a significant paradox: the parameters that improve mechanical strength, such as increased layer adhesion and infill density, frequently compromise the aesthetic and functional quality of the surface finish. Closing this gap requires purposeful optimisation rather than repetitive conjecture. As a result, the discipline has unified around a sophisticated statistical toolkit that utilises structured design of experiments (DOE) and resilient response modelling. Researchers carefully analyse this intricate interaction using techniques such as Taguchi screening, complete and fractional factorial designs, and the predictive power of response surface methodology (RSM). These methodologies surpass mere parameter adjustment; they measure causal effects through ANOVA and develop empirical models to identify the exact operational optimal

Table 1. Summary of key FDM parameters evaluated for PETG

Parameter	Typical range reported	Main observed effect	Representative findings
Layer height	0.06–0.30 mm	Strong control of surface roughness; finer layers tend to improve tensile strength after annealing	Layer height explained ~82% of roughness variance and 13–> significant effect on tensile strength in separate studies [3,12,16]
Infill density & pattern	20–100% density; patterns: gyroid, grid, zig-zag, triangle	Higher density increases UTS; pattern strongly influences load paths and strength (gyroid often best)	Infill geometry accounted for ~63.6% effect on tensile strength; gyroid outperformed zig-zag/grid/triangle for UTS in one Taguchi study [12]
Nozzle/extrusion temp	220–250 °C	Higher nozzle temps generally increase interlayer bonding and UTS within studied ranges	Tensile strength increased up to ~250 °C in multiple studies; typical optimum around 240–250 °C reported [4,12]
Printing speed	30–80 mm/s	Higher speed can reduce filament fusion and lower strength; effect magnitude variable	Studies report speed as a secondary factor compared with temperature and infill
Build orientation & raster angle	0°–90° relative to load	Dominant influence on anisotropy and failure location; flat/print-along tensile axis improves apparent UTS	Build/orientation included among five key parameters affecting tensile behavior in statistical models [4]
Bed temperature	Ambient to ~90 °C	Influences warping, dimensional stability and first-layer adhesion; warmer beds reduce curl	Bed temperature used to control dimensional accuracy and first-layer bonding in experimental setups [4]
Cooling/part fan	Off to 100%	Can affect crystallinity and interlayer fusion; low cooling often favors PETG bonding	Fan speed was found to have minor effect on tensile in one Taguchi study (≈2.7%) but can influence surface solidification [12]
Postprocessing / annealing	60–100 °C for 30–90 min	Can increase modulus and UTS and reduce internal stresses; interacts strongly with layer height	Optimal annealing combos improved PETG UTS and reduced dimensional change in multi-factor study [16]

point where durability aligns with refinement, converting a technical compromise into a manageable engineering result (Table 2).

Although previous research has successfully employed DOE and RSM to analyse the distinct effects of printing parameters on the surface quality and mechanical strength of PETG, a significant, application-focused gap remains. Numerous studies regard the two critical performance outcomes, surface quality and tensile integrity, as distinct, concurrent optimisation objectives, frequently resulting in isolated "optimal" parameter configurations that may be inconsistent. In practical engineering, components are never evaluated based on a singular criterion; they necessitate a harmonious performance profile customised to particular functional and aesthetic requirements. This study presents an innovative dual-outcome optimisation framework that directly addresses this disparity. This study transcends singular optima by methodically examining and modelling the causal link between surface roughness (affected by core parameters such as layer height) and tensile strength (determined by structural elements like infill pattern). This framework is not merely an additional parameter screening method; it is a predictive approach that elucidates how parameter selections simultaneously impact both surface properties and mechanical performance. This enables users to traverse the trade-off landscape adeptly, facilitating the selection of printing parameters tailored not for a universal optimum, but for a bespoke performance profile, emphasizing extreme strength, impeccable finish, or a specific equilibrium of both, thus converting generalised process guidelines into a decision-support instrument for functional part design.

MATERIALS AND METHODOLOGY

Materials

This research utilises PETG thermoplastic polyester in FDM. The PETG filament manufactured by Prusa Research, by Josef Prusa exhibits excellent mechanical qualities. The PETG material utilised is in Jetblack colour and features a filament diameter of 1.75 mm with a tolerance of 0.02 mm. Table 3 presents the printing setup for this specific PETG Prusament.

Table 2. Summary of statistical toolkit for FDM parameters optimization

Method	Purpose	Representative studies
Taguchi L16	Efficient screening and ranking of multi-factor influence (4 factors × 4 levels common)	Multiple studies used Taguchi for tensile and roughness optimization and reported effect-size percentages for parameters [3,12,15]
Response surface method (RSM) / regression	Develop predictive models and find continuous optima with interaction terms	Regression models used to relate layer height and annealing to tensile outcomes with validation errors ≈5% in one study [16]
ANOVA	Statistical significance testing and effect size estimation	ANOVA used alongside Taguchi and RSM to identify dominant parameters and interactions in tensile/ roughness studies [4,12]
FEM and specimen geometry studies	Assess stress distributions and failure initiation to improve test repeatability	Comparative study on specimen geometries and slicer approaches recommended standardized methods for effective property measurement [17]

Table 3. Normal printing setup for PETG Prusament

NozzleTemperature	250 ±10 °C
Heatbed Temperature	80 ±10 °C
Recommended Steel Sheet	Textured / Satin

FDM printer specification

The selection of a 3D printer depends on its compatibility with specific filament materials and the range of process parameters available for experimental evaluation. This research utilised a PRUSA I3 MK3S+ 3D printer, selected for its accuracy, dependability, and customisable parameter settings. A fundamental requirement for printing PETG is the hot end's ability to exceed the material's melting temperature, which is met by the printer's maximum nozzle temperature of 300 °C. Additionally, a heated build plate is crucial for ensuring proper layer adhesion and reducing warping. The printer is equipped with a heated bed that can sustain temperatures within the ideal range for PETG. Prusament PETG Jet Black filament was employed for all specimens due to its uniform diameter and material characteristics. Ultimately, due to the likelihood of material wear over prolonged usage, the printer's employment of conventional, easily accessible V6-style brass nozzles enables uncomplicated maintenance and replacement, thereby ensuring consistent printing throughout the experimental campaign.

Design of experiment using RSM

To scrutinize the paraphernalia of printing parameters on surface quality, surface roughness was selected as the measured response and assessed in accordance with the ISO 4288 standard. An RSM approach was adopted to structure the experiment. A three-factor DOE was implemented, with nozzle temperature, bed temperature, and layer height defined as the independent variables, as visualized in Figure 1. The selection of factor levels for the DOE was based on a combination of the material manufacturer's recommendations and empirical ranges established in prior PETG FDM studies. The range of 240–260 °C for the nozzle temperature and 70–90 °C for the bed temperature was chosen as it encompasses the recommended printing temperature for the specific Prusament PETG Jet Black filament (per datasheet: 250±10 °C for nozzle temperature and 80±10 °C for bed temperature) while allowing investigation of under- and over-temperature effects. These factors, along with their corresponding low (-1), center (0), and high (+1) levels, are detailed in Table 4 and were used as inputs for analysis in Design-Expert® software to generate a set of 20 experimental runs.

The FDM method commences with the digital design of the specimen. A rectangular test coupon measuring 25.0 × 25.0 × 2.4 mm was created utilising computer-aided design (CAD) software. The three-dimensional model was subsequently exported in the standard tessellation language (STL) file format, which depicts the object's surface geometry as a mesh of interlinked triangles. The STL file was thereafter imported into specialised slicing software. In this software, essential production parameters, including layer height, print speed, infill pattern, and density, and

Table 4. Parameter correspondence level

Parameter	Level		
	-1	0	1
Nozzle temperature (˚C)	225	235	245
Bed temperature (˚C)	70	80	90
Layer height (mm)	0.15	0.175	0.2

build plate adhesion settings, were established. The slicer algorithmically divides the model into distinct horizontal levels and produces toolpath instructions, encompassing extrusion trajectories and temperature controls, which are assembled into a machine-readable G-code file. This G-code governs the physical printing procedure, in which a thermoplastic filament is supplied to a heated extrusion nozzle. The material is liquefied and selectively applied in layers onto a build platform following the designated trajectory. Subsequent to deposition, the material swiftly hardens, adhering to the prior layer to progressively construct the ultimate three-dimensional component (Figure 2, Table 5).

Surface roughness and tensile test

The experimental methodology began with the implementation of a structured DOE. The specimen printing parameters were obtained from the experimental matrix created by Design-Expert® software. After manufacture, the surface roughness (Ra) of each specimen was quantitatively evaluated using a Mitutoyo Surf Test SJ-210 Series 178 Portable Surface Roughness Tester (profilometer). Measurements were performed with the instrument's integrated standard diamond stylus (tip radius: 5 µm) under its default measuring force of 4 mN (0.4 gf). In accordance with ISO 4288 standards for additively manufactured surfaces, a cut-off length (λc)

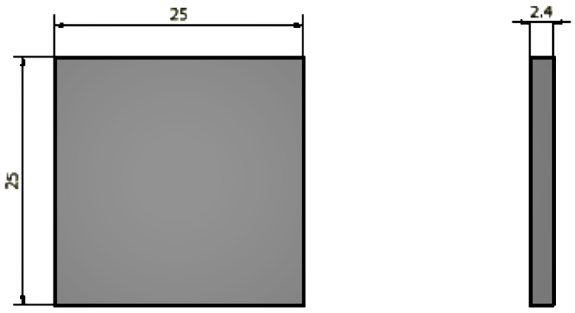

Figure 2. Size of the specimens

of 0.8 mm was selected. The evaluation length was 4.0 mm (5 × λc), and the traverse length was 6.4 mm. Each reported Ra value is the arithmetic mean of five separate measurements taken along the gauge length of each specimen. The instrument's calibration certificate confirms a measurement accuracy of ±5% of reading for the specified range. To guarantee statistical reliability and address potential directional anisotropy associated with the FDM process, five distinct measurements were conducted along the 0° build direction (designated as $Ra_{,0}$) and an additional five along the 90° direction (designated as $Ra_{,90}$) for each specimen, as depicted in Figure 3. All measured values were exhibited on the device's LCD screen and subsequently sent and documented on a connected computer for analysis. The obtained surface roughness data were subsequently input into the Design-Expert® software for statistical modelling and optimisation. An ANOVA was conducted to ascertain the significance of each printing parameter and to establish the ideal combination for reducing surface roughness. ANOVA systematically partitions the overall variation in the response data into components associated with the controlled factors (nozzle temperature, bed temperature, layer height) and unexplained experimental error, facilitating the evaluation of each parameter's impact.

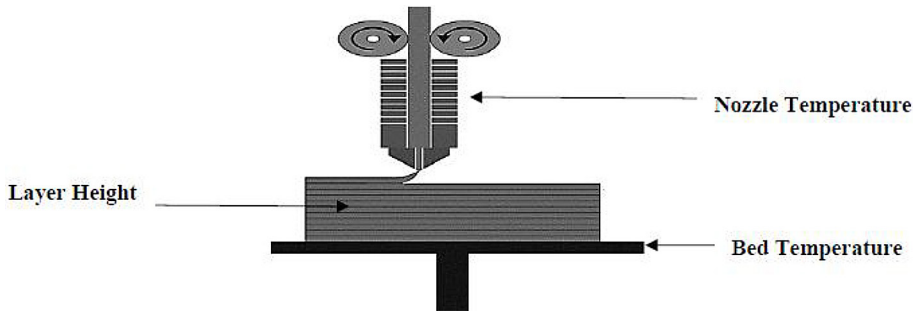

Figure 1. Independent factor parameters

Table 5. Fixed printing parameters

Fixed parameter	Value
Volumetric flow rate	8 mm^3/s
Nozzle diameter	0.4 mm
Fan speed	0%
Print speed	90 mm/s
Fill density	100%
Travel speed	150 mm/s
Fill pattern	Rectilinear

The characteristics of these influences and the interrelations among parameters were modelled utilising RSM. The amalgamation of ANOVA and RSM enabled an exhaustive investigation, allowing for the discovery of critical elements, the formulation of a predictive model for surface roughness, and the numerical optimisation of printing settings.

Tensile test specimens were produced utilising the identical fixed printing parameters established for the surface roughness investigation to maintain process consistency. The geometry of the tensile specimens adhered to the ASTM D638 standard (Standard test method for tensile properties of plastics) with specific dimensions depicted in Figure 4. The manufacturing process entailed creating a solid model in computer-aided design (CAD) software, exporting the model to PrusaSlicer for G-code generation with specified parameters as illustrated in Figure 5, and executing final fabrication with an FDM 3D printer utilising 1.75 mm diameter PETG filament. To assess the impact of interior structure on mechanical performance, all tensile specimens were fabricated with a 100% infill density. A 100% infill density was utilized to evaluate the maximum potential tensile strength and failure characteristics of each pattern topology, minimizing the variable of porosity. This establishes a controlled baseline essential for isolating the geometric contribution of the infill pattern, though it is recognized that practical applications often employ lower densities for material efficiency. According to the results of the surface roughness optimisation, the determined optimal parameter set (nozzle temperature, bed temperature, layer height) was chosen to fabricate specimens with the highest attainable surface quality. A comparative mechanical investigation was performed using ideal parameters by fabricating specimens with three different infill patterns: concentric, octagram spiral, and rectilinear, as illustrated in Figures 6 (a), (b), and (c), respectively. To guarantee statistical reliability, five identical replicates were produced and evaluated for each infill pattern configuration.

Tensile testing was conducted with a universal testing machine (Instron 3369). All tests were performed at ambient temperature with a uniform crosshead displacement rate of 2 mm/min and a maximum load cell capacity of 50 kN. Throughout each test, the machine's integrated data acquisition system captured load, extension, strain, and time data in real-time. Key mechanical parameters, including ultimate tensile strength, yield strength, Young's modulus, and fracture strain, were derived from the raw data to assess the performance of each specimen. In this study, ultimate tensile strength (UTS) is defined as the maximum engineering stress sustained by the specimen before fracture. Yield strength was determined using the 0.2% offset method applied to the engineering stress-strain curve, in accordance with ASTM D638. This method involves drawing a line parallel to the initial linear elastic portion of the curve, offset by a strain of 0.002, with the intersection of this line and the stress-strain curve defining the yield point. Figure 7 displays the manufactured ASTM D638 specimen before mechanical testing and Figure 8 shows the fracture condition of the specimens after the tensile testing.

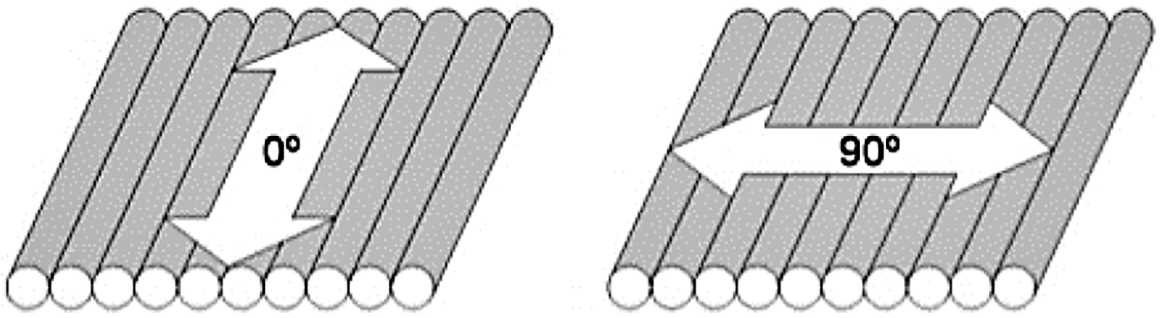

Figure 3. Graphical explanation for measurement [13]

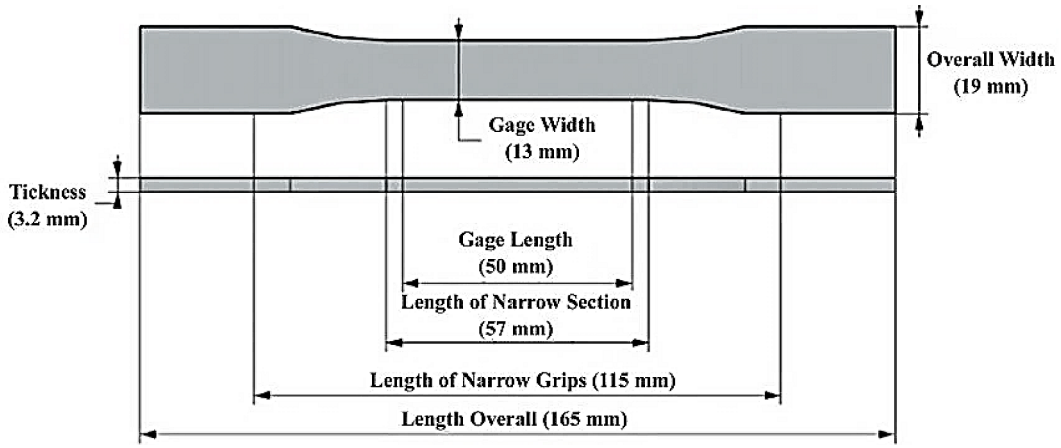

Figure 4. Dimensions of ASTM D638

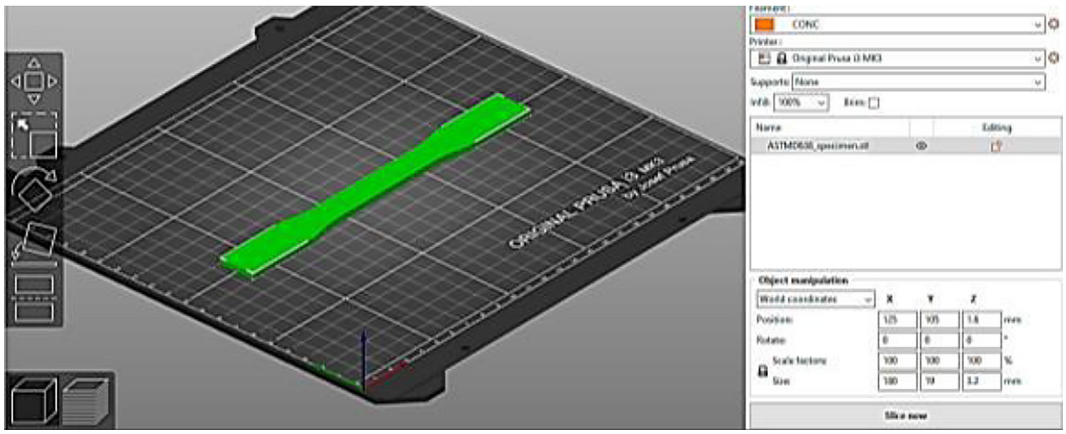

Figure 5. ASTM D638 in Prusa slicer

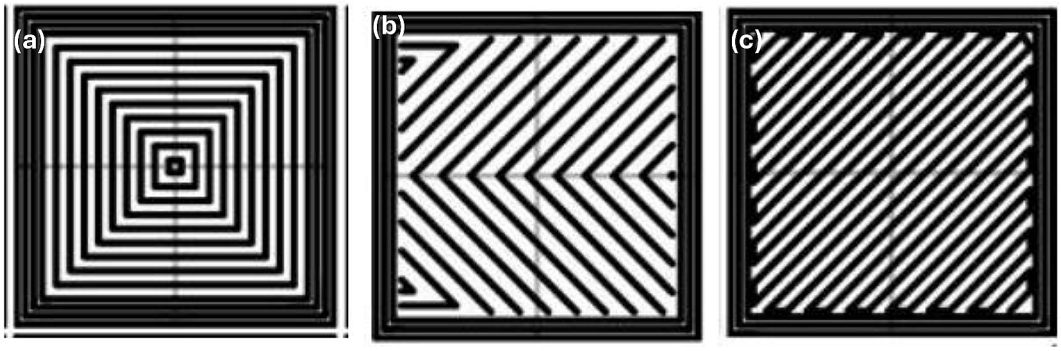

Figure 6. Infill pattern: (a) concentric, (b) octagram spiral, and (c) rectilinear

RESULTS AND DISCUSSION

Surface roughness test by DOE

Table 6 presents the measured surface roughness results for both the 0° and 90° orientations. These data pertain to the 20 experimental trials established by the RSM design. To enhance measurement reliability, the reported Ra value for each specimen is the average of five separate profilometer measurements, thus minimising random error. For 0° direction, the minimum surface roughness of 1.7564 µm was achieved in Run 2, utilizing a nozzle temperature of 240 °C, a 90 °C bed temperature and a 0.20 mm layer height. Conversely, the maximum roughness for this orientation was recorded at 5.8140 µm in Run 18

Figure 7. ASTM D38 Specimen. (a) Concentric, (b) Octagram spiral, (c) Rectilinear

Figure 8. ASTM D638 Specimen after Tensile test. (a) Concentric, (b) Octagram spiral, (c) Rectilinear

at 260 °C, 80 °C, and 0.175 mm, respectively. For the measurements taken in the 90° direction, the minimum roughness was observed to be 6.2856 µm in Run 1, under the parameters of 250 °C, 80°C, and 0.175 mm. The maximum roughness for this direction reached 11.7010 µm in Run 6, utilising settings of 260 °C, 90 °C, and a layer height of 0.15 mm; these values are indicated in green within the table. An ANOVA was subsequently conducted to statistically validate the significance of the reported impacts of the printing settings.

Analysis of variance (ANOVA) for surface roughness direction 0° (Ra 0°) and direction 90° (Ra 90°)

The primary objective of this investigation was to determine the key printing parameters that influence surface roughness. In this orientation, the p-values related to factor A (nozzle temperature), factor B (bed temperature), and factor C (layer height) all surpassed the conventional significance threshold of $\alpha = 0.05$. P-values greater than 0.05 suggest that the observed fluctuations associated with these factors lack statistical significance, indicating they are likely the result of random error rather than a systematic influence. Thus, throughout the examined parameter ranges, none of these individual parameters exhibited a significant effect on the surface roughness recorded at 0°. This indicates that other, unassessed variables or experimental noise may significantly influence the results in this particular direction. Despite Figures 9 and 10 indicating an optimal parameter combination (240 °C nozzle temperature, 90 °C bed temperature, and 0.15 mm layer height), this numerical prediction lacks statistical validation from the model. The regression model for the 0° direction surface roughness is deemed inaccurate due to the absence of substantial model terms, rendering its predictions unsuitable for optimisation.

The ANOVA model for surface roughness evaluated at the 90° direction was statistically significant, with a model p-value of 0.03388 ($\alpha = 0.05$). An analysis of the individual factor p-values indicates that layer height ($p = 0.0349$) was significant, although bed temperature ($p = 0.0587$) and nozzle temperature ($p = 0.2160$) were not significant at the 0.05 level. Consequently, within the evaluated design parameters, layer height emerged as the principal factor markedly affecting surface roughness in the 90° orientation. Figure 11 graphically substantiates this discovery, demonstrating that optimal surface

Table 6. Result for surface roughness test (Ra,0°, Ra,90°)

Std	Run	Block	Factor 1: Nozzle temperature (◦C)	Factor 2: Bed temperature (◦C)	Factor 3: Layer height	Response1: Ra, 0° (µm)	Response 2: Ra, 90° (µm)
15	1	Block 1	250	80	0.175	2.2024	6.2856
7	2	Block 1	240	90	0.2	1.7564	13.9312
6	3	Block 1	260	70	0.2	5.1350	10.0664
13	4	Block 1	250	80	0.15	5.7704	7.2746
9	5	Block 1	240	80	0.175	5.0458	7.4668
4	6	Block 1	260	90	0.15	4.3078	11.7010
18	7	Block 1	250	80	0.175	3.7828	7.7114
1	8	Block 1	240	70	0.15	4.6018	7.5376
17	9	Block 1	250	80	0.175	3.9866	8.2020
2	10	Block 1	260	70	0.15	4.3042	7.5140
12	11	Block 1	250	90	0.175	4.1550	7.6368
3	12	Block 1	240	90	0.15	4.9552	6.704
8	13	Block 1	260	90	0.2	5.6462	11.0746
5	14	Block 1	240	70	0.2	3.8172	7.7290
14	15	Block 1	250	80	0.2	4.0936	9.5764
16	16	Block 1	250	80	0.175	3.2124	9.4684
20	17	Block 1	250	80	0.175	5.4600	8.5066
10	18	Block 1	260	80	0.175	5.8140	9.5216
11	19	Block 1	250	70	0.175	4.5180	7.9056
19	20	Block 1	250	80	0.175	4.7476	6.8634

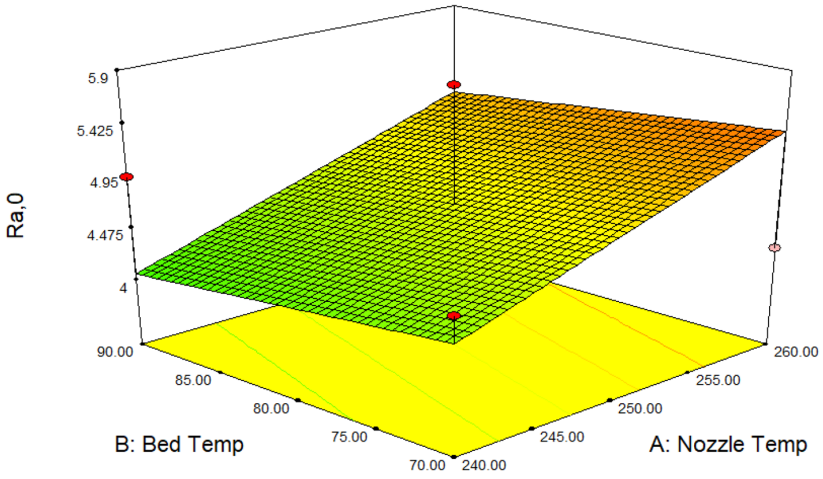

Figure 9. Bed temperature vs nozzle temperature graph for Ra,0°

roughness is attained with minimal layer height with reduced bed and nozzle temperatures, which is consistent with previous work [18]. Similarly determined that reducing layer height is essential for decreasing surface roughness in FDM processes. The numerical optimisation in the model determines that a parameter set of 0.15 mm layer height, 240 °C nozzle temperature, and 70 °C bed temperature produces the anticipated optimal surface finish for this orientation (Figure 12).

The analysis demonstrates a basic directional anisotropy in the impact of printing parameters on surface roughness. The model demonstrated statistical significance in the 90° direction ($p = 0.03388$) but not in the 0° direction, highlighting a crucial observation: the influence of nozzle temperature, bed temperature, and layer height is not uniform but is significantly contingent upon the measurement orientation in relation to the printing direction. The absence of significance in the 0° direction model constitutes a significant constraint. This indicates that within the selected parameter ranges, these factors do not consistently regulate roughness in that

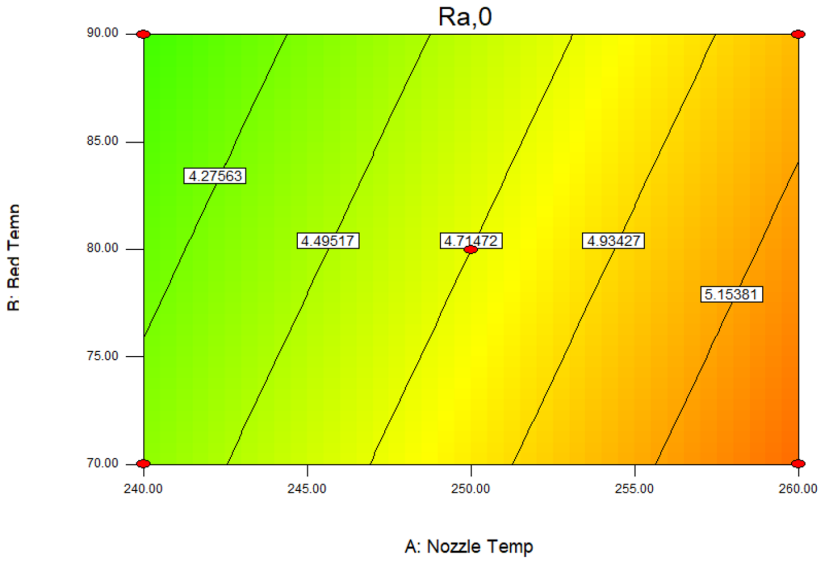

Figure 10. Interaction between bed temperature and nozzle temperature in contour view (Ra, 0°)

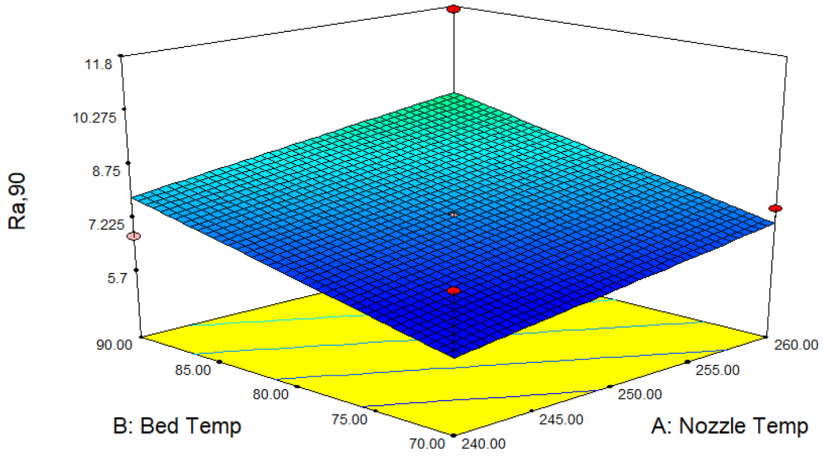

Figure 11. Bed temperature vs nozzle temperature graph for Ra, 90°

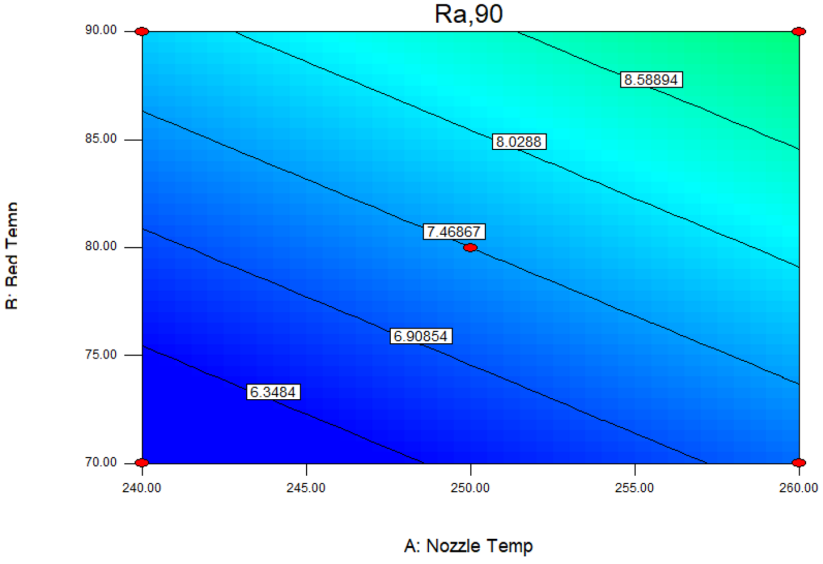

Figure 12. Interaction between bed temperature and nozzle temperature in contour view (Ra, 90°)

orientation, either due to predominant noise from other unaccounted variables (e.g., vibration, filament consistency) or an inadequately large effect size. This constrains the model's predictive capability and general application across all surface orientations, which is a vital factor for intricate components.

Statistical analysis for the 90° direction confirms that the layer height is the only significant factor influencing surface roughness, with $p = 0.0349$. Bed temperature ($p = 0.0587$) is minimal and should be considered a potentially relevant factor rather than a conclusively contributing one. The statistical analysis indicates that layer height and bed temperature exert the most significant influence on the observed surface roughness. This accuracy is crucial for effective knowledge transfer. The outcome is consistent with existing theory, indicating that reduced layer heights diminish stair-stepping effects, and is further supported by agreement with Pérez [18], enhancing external validity.

Tensile-yield strength

The ANOVA results, as outlined in the methodology section (surface roughness and tensile test), were utilised to establish the printing settings for the tensile (dog bone) specimens. The parameter selection was exclusively determined by the investigation of the 90° surface roughness direction, as the model for the 0° direction was statistically insignificant. This result is a constraint of the present experimental design, which did not capture a significant effect value for the 0° orientation within the chosen parameter space. It does not preclude the existence of such relationships but defines a clear boundary for the current model's applicability and a focal point for future work. Accordingly, the specimen printing conditions were established with a layer height of 0.15 mm, a nozzle temperature of 240 °C, and a bed temperature of 70 °C.

Figure 13 illustrates that both ultimate tensile strength (UTS) and strain at break are significantly influenced by the infill geometry. The concentric demonstrated exceptional performance, with the highest mean ultimate tensile strength (41.4 MPa) and strain (4.4388%). This outcome is ascribed to its continuous, contour-oriented deposition trajectory, which optimally aligns filament layers with the applied tensile load, thus reducing interlayer separation and enhancing uniform stress distribution [19]. Conversely, the rectilinear pattern yielded a reduced ultimate tensile strength of 32.7 MPa and a strain of 3.585%. The distinctive alternating 0°/90° raster orientation results in just a fraction of the deposited routes being perfectly aligned with the tensile axis, leading to inherent stress concentrations and diminished overall efficacy. The octagram spiral configuration had the lowest mechanical parameters, featuring a UTS of 28.9 MPa and a strain of 2.9396%. This inadequate performance arises from its discontinuous, radial geometry, which causes the structural layers to be susceptible to separation under tension, resulting in premature failure [20]. The maximum UTS is consistently linked to the infill pattern that achieves optimal alignment between the filament deposition trajectory and the major tensile stress

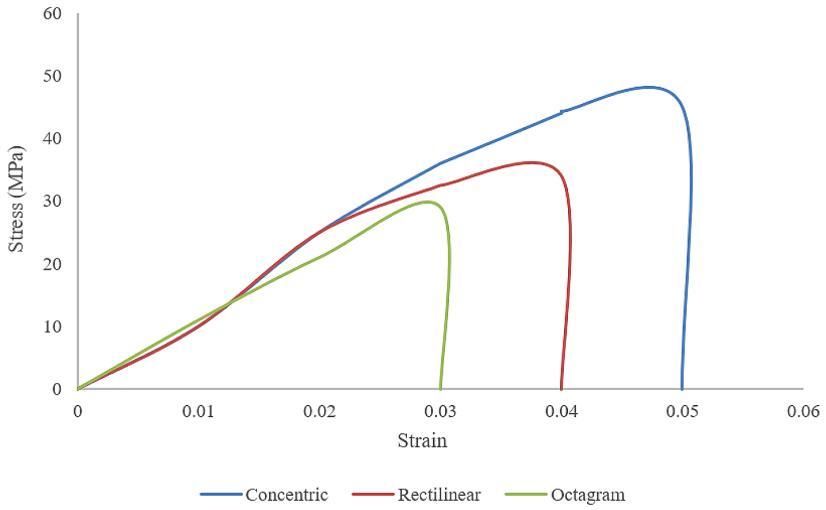

Figure 13. Tensile strength of the PETG specimen with respect to three infill patterns

direction, determined by the effective layer orientation during manufacturing [21].

The findings further demonstrate that yield strength exhibits the same trend as shown in Figure 14, being substantially affected by the infill design and its corresponding effective build orientation, as shown in Figure 14. The concentric design had the greatest yield strength (32.7 MPa), followed by the rectilinear (27.4 MPa) and octagram spiral (22.9 MPa) patterns. This hierarchy is directly related to the orientation of deposited layers concerning the tensile stress axis (Z-axis, as illustrated in Figure 14). The concentric configuration, with a nominal layer orientation of 90° to the build plate (see Figure 15), ensures optimal alignment with the applied load as shown in Figure 16. The rectilinear pattern, orientated at 45°, provides only partial alignment, whilst the octagram spiral pattern, orientated at 0°, results in the least favourable alignment, causing diminished load-bearing capacity and premature yielding. Thus, yield strength is optimised when the effective construction orientation is at a 90° angle to the tensile axis. This verifies that the geometric configuration dictated by the infill pattern, particularly the angle between laid roads and the load direction, is the primary determinant of yield performance, regarding build orientation as a crucial process parameter [22].

The study's primary merit is its explicit, quantitative illustration of a performance hierarchy among infill types. The data strongly corroborates the conclusion that the concentric pattern produces the maximum ultimate tensile strength (41.4 MPa), yield strength (32.8 MPa), and ductility (4.44%

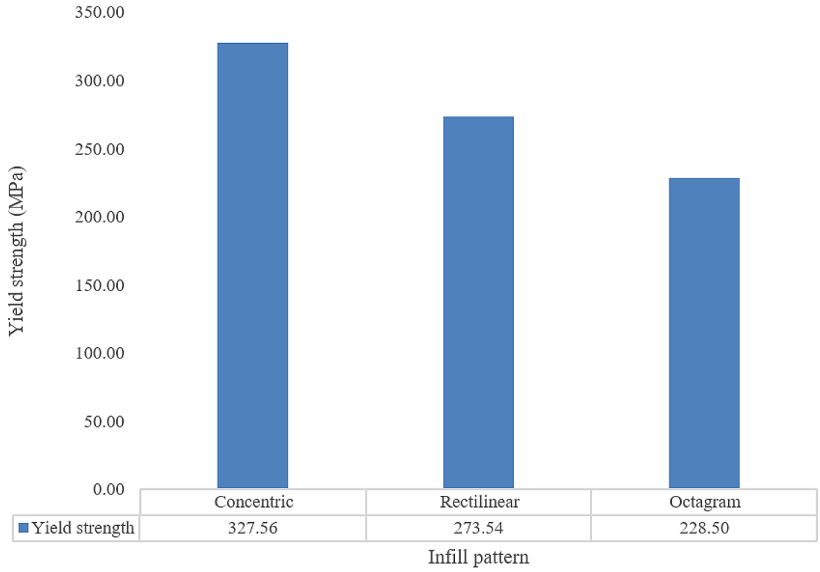

Figure 14. Yield strength of the PETG specimen with respect to three infill patterns

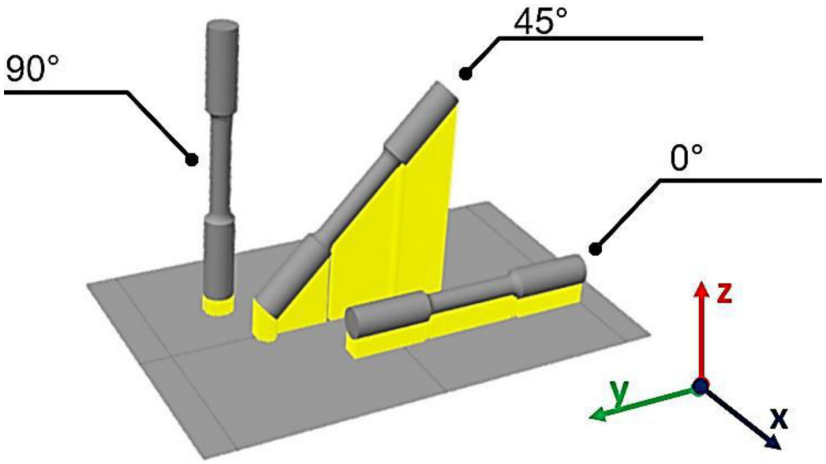

Figure 15. Build orientation for the PETG specimen

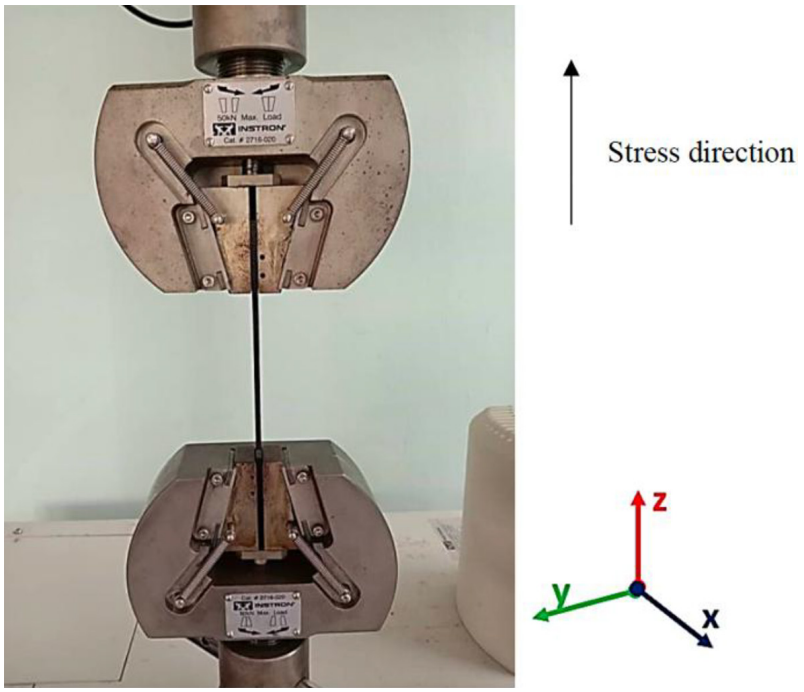

Figure 16. Stress direction for the PETG specimen

strain). The association of this exceptional performance with advantageous layer alignment (about 90° to the load axis) is substantiated by composite mechanics theory. The recognition of the rectilinear pattern as the optimal compromise, which is supported by the printing time vs material consumption graph presented in Figure 17, delivering adequate strength with reduced material consumption and printing duration, offers essential practical guidance for engineers, emphasising resource efficiency rather than maximum performance. The research identifies a significant trade-off: the concentric design, although the most robust, utilises the least material (3.86 m) and has the shortest printing duration (49 min), establishing a performance benchmark. The rectilinear pattern necessitates merely 2% additional material and 8% extra time compared to the concentric design, while providing significantly greater tensile strength than the octagram spiral, which incurs the longest printing duration without any advantages in material efficiency or strength. The correlation between UTS and yield strength trends enhances the internal validity of the findings, affirming that infill geometry significantly influences both elastic and plastic deformation behaviour.

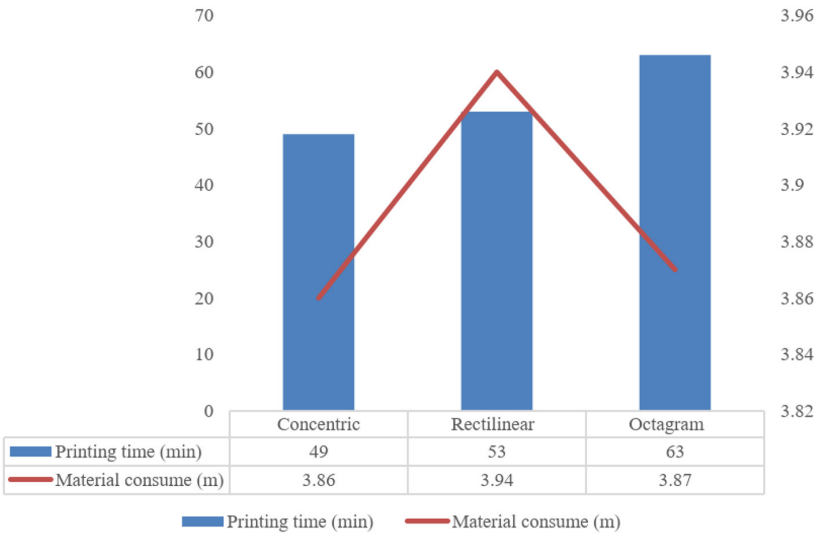

Figure 17. Printing time vs material consumption graph for each infill pattern

CONCLUSIONS

This study presents two significant, verified discoveries that enhance the comprehension of PETG FDM. A fundamental directional anisotropy is present: layer height significantly influences surface roughness perpendicular to the print direction (90°), however, the examined parameters did not produce a significant model for in-layer roughness (0°). Secondly, mechanical performance is determined by a distinct relationship, wherein the type of infill pattern, rather than surface parameters, serves as the primary influence on tensile strength. The results furnish a mathematical foundation for application-specific decision-making: practitioners may prioritise minimal layer heights for smooth vertical surfaces, opt for concentric infill to maximise strength, and employ rectilinear infill to achieve an efficient balance of attributes. A key methodological restriction is the limited statistical power of the 0° surface roughness model, which confines its predictive capacity for that particular orientation. The study also concentrated on parameter interactions at a constant 100% infill density, restricting direct extrapolation to lightweight, efficiency-oriented applications.

The primary innovation of pursuing a dual-outcome optimisation paradigm is praiseworthy. Nevertheless, the data elucidate its intricacy. The "optimal" parameter for surface finish, such as reduced layer height, may vary from the ideal configurations for enhancing mechanical integrity, which may rely more on infill and adhesion. The practical utility of the "prediction system" depends on its capacity to openly quantify these trade-offs. The current results establish a basis by demonstrating specific parameter impacts on roughness and autonomous infill effects on strength. The journey to mastering PETG in FDM involves strategically navigating intrinsic and anisotropic trade-offs rather than seeking a universal "best setting". The results reveal a fundamental truth: surface quality and mechanical performance are determined by separate, and frequently conflicting, process-property relationships.

This work's contribution is not a universal optimum, but rather a shown and quantified decision-making framework. By elucidating these discrete process-property relationships, where surface quality, mechanical strength, and printing efficiency are dictated by unique and frequently opposing parameters, it imparts essential knowledge for prioritising among competing factors. This shifts practice from broad guidelines to performance-oriented manufacturing. This framework logically progresses towards the development of a full multi-objective model, essential for sophisticated predictive tools in FDM.

To directly mitigate the limitation of limited statistical power in the 0° direction model and to enhance the suggested optimisation framework, future research should concentrate on broadening the experimental parameter space. A principal objective is to execute a follow-up investigation utilising an enhanced design of experiments that encompasses a broader spectrum of layer heights, printing velocities, and cooling rates. This would augment the effect size and strengthen the model's robustness for both surface orientations. Moreover, to achieve a holistic multi-objective optimisation system, future research must incorporate additional essential parameters beyond surface roughness and tensile strength, such as dimensional accuracy (shrinkage/warping), into a cohesive predictive model. This progression is crucial for creating the authentic digital twin of the FDM proposed here, which can accurately forecast the unique balance of characteristics required for functional components.

Acknowledgment

The authors express their gratitude to the Centre for Research Excellence and Incubation Management, CREIM, Universiti Sultan Zainal Abidin, for generously giving financial support and research facilities through research grant UNISZA/2024/DPU2.0/17 to carry out this study.

REFERENCES

1. Khan S, Joshi K, Deshmukh S. A comprehensive review on effect of printing parameters on mechanical properties of FDM printed parts. Mater Today Proc 2022;50:2119–27.
2. El Omari A, Ouballouch A, Nassraoui M. Optimising surface roughness, dimensional accuracy and printing time of FDM PETG parts using statistical methods and artificial neural network. Archives of Materials Science and Engineering 2025;133:5–17. https://doi.org/10.5604/01.3001.0055.2924
3. Shabeeb A.H, Abdulwahhab A.B, Ismael H.S, Ghazi S.K. Optimization of fused deposition modeling parameters to enhance tensile strength and surface roughness of polyethylene terephthalate

glycol. Advances in Science and Technology Research Journal 2025;19:345–58. https://doi.org/10.12913/22998624/205716

4. Ranganathan S, Palanivelu R. Enhancing the tribological properties PETG and CFPETG composites fabricated by FDM via various infill density and annealing. SAE Technical Paper; 2020.
5. Holcomb G, Caldona E.B, Cheng X, Advincula R.C. On the optimized 3D printing and post-processing of PETG materials. MRS Commun 2022;12:381–7. https://doi.org/10.1557/s43579-022-00188-3
6. Kumaresan R, Kadirgama K, Samykano M, Harun W.S.W, Thirugnanasambandam A, Aslfattahi N, et al. Optimization of inter-layer printing parameters for enhanced mechanical performance of PETG in Fused Deposition Modeling (FDM). Results in Engineering 2025;25:104564. https://doi.org/https://doi.org/10.1016/j.rineng.2025.104564
7. Djurovic S, Velikinac N, Ivkovic M, Lazarević D, Mišić M, Stojčetović B, et al. Influence of layer height on the surface roughness of FDM printed PETG parts. 40th International Conference On Production Engineering-Serbia 2025, Faculty of Mechanical Engineering-University of Nis; 2025.
8. Sapkota A, Ghimire S.K, Adanur S. Effect of FDM process parameters on mechanical properties of 3D-printed fabrics and yarns from polyethylene terephthalate glycol, nylon and thermoplastic polyurethane. Rapid Prototyp J 2025;31:934–49. https://doi.org/10.1108/RPJ-08-2024-0338.
9. Kumaresan R, Kadirgama K, Samykano M, Harun W.S.W, Thirugnanasambandam A, Kanny K. In-depth study and optimization of process parameters to enhance tensile and compressive strengths of PETG in FDM technology. Journal of Materials Research and Technology 2025;37:397–416. https://doi.org/https://doi.org/10.1016/j.jmrt.2025.06.013
10. Valvez S, Silva A.P, Reis P.N.B. Optimization of printing parameters to maximize the mechanical properties of 3D-printed PETG-based parts. Polymers (Basel) 2022;14:2564.
11. Taqdissillah D, Mutaqqin A.Z, Darsin M, Dwilaksana D, Ilminnafik N. The effect of nozzle temperature, infill geometry, layer height and fan speed on roughness surface in PETG filament. Journal Mechanical Engineering Science and Technology (JMEST) 2022;6:74–84.
12. Srinivasan R, Ruban W, Deepanraj A, Bhuvanesh R, Bhuvanesh T. Effect on infill density on mechanical properties of PETG part fabricated by fused deposition modelling. Mater Today Proc 2020;27:1838–42. https://doi.org/https://doi.org/10.1016/j.matpr.2020.03.797
13. Özen A, Auhl D, Völlmecke C, Kiendl J, Abali B.E. Optimization of manufacturing parameters and tensile specimen geometry for fused deposition modeling (FDM) 3D-printed PETG. Materials 2021;14:2556.
14. Stojković J.R, Turudija R, Vitković N, Górski F, Păcurar A, Pleşa A, et al. An experimental study on the impact of layer height and annealing parameters on the tensile strength and dimensional accuracy of FDM 3D printed parts. Materials 2023;16. https://doi.org/10.3390/ma16134574
15. Mardlotila M.J, Trifiananto M, Dwilaksana D, Basuki H.A, Kustanto M.N, Hardiatama I. Effect of layer height, infill geometry, nozzle temperature, and fan speed on tensile strength of 3D printing PETG specimens. INVOTEK: Jurnal Inovasi Vokasional Dan Teknologi 2022;22:149–58.
16. Clarke T, Hosseini A. Effects of print parameters on tensile characteristics of additively manufactured polyethylene terephthalate-glycol (PETG). The International Journal of Advanced Manufacturing Technology 2023;125:4953–74. https://doi.org/10.1007/s00170-023-11003-1
17. Kumaresan R, Samykano M, Kadirgama K, Pandey A.K, Rahman Md.M. Effects of printing parameters on the mechanical characteristics and mathematical modeling of FDM-printed PETG. The International Journal of Advanced Manufacturing Technology 2023;128:3471–89. https://doi.org/10.1007/s00170-023-12155-w
18. Pérez M, Medina-Sánchez G, García-Collado A, Gupta M, Carou D. Surface quality enhancement of fused deposition modeling (FDM) printed samples based on the selection of critical printing parameters. Materials 2018;11:1382.
19. Rudrakotti A.R.B, Palanivel K, Nagarajan P, Manjunathan K, Dillibabu S.P, Megaraj M. The impact of infill patterns on the mechanical and surface characteristics of PETG material in 3D printing. AIP Conf Proc 2024;3192:020084. https://doi.org/10.1063/5.0241970
20. Panneerselvam T, Raghuraman S, Vamsi Krishnan N. Investigating mechanical properties of 3D-printed polyethylene terephthalate glycol material under fused deposition modeling. Journal of The Institution of Engineers (India): Series C 2021;102:375–87.
21. Mahesh E.U, Narayana Y.V, Sridhar B. Investigations of influence of infill pattern on tensile strength of 3D-printed poly lactic acid and polyethylene terephthalate glycol material using design of experiments. Mater Today Proc 2023. https://doi.org/https://doi.org/10.1016/j.matpr.2023.03.406
22. Baharudin M.E, Saad M.S, Zakaria M.Z, Nor A.M, Ab Talib M.H. FDM parameters optimization for improving tensile strength using response surface methodology and particle swarm optimization. Journal of Advanced Research in Applied Sciences and Engineering Technology 2024;38:112–28.